Low temperature Al_2O_3 surface passivation for carrier-injection SiGe optical modulator

Younghyun Kim,* Jaehoon Han, Mitsuru Takenaka, and Shinichi Takagi

Dept. of Electrical Engineering and Information Systems, The University of Tokyo, 7-3-1 Hongo, Bunkyo-ku, Tokyo 113-0032, Japan

yhkim@mosfet.t.u-tokyo.ac.jp

Abstract: Surface passivation by Al_2O_3 deposited by atomic layer deposition (ALD) at 200 °C is examined to suppress surface recombination for carrier-injection SiGe optical modulators. We have investigated the interface trap densities at SiO_2/Si and Al_2O_3/Si interfaces formed by plasma enhanced chemical vapor deposition (PECVD) and ALD, respectively. By evaluating metal-oxide-semiconductor (MOS) capacitors formed on Si surfaces after dry etching, we found that the interface trap density of Al_2O_3 passivated surface is more than one order of magnitude less than that of SiO_2 passivated one. As a result, the modulation efficiency is improved by 1.3 by inserting Al_2O_3 layer prior to SiO_2 deposition by PECVD owing to superior interface between Al_2O_3 and Si. The Al_2O_3 passivated device exhibits comparable modulation efficiency to a thermally-grown SiO_2 passivated one formed by dry oxidation. Hence, the ALD Al_2O_3 passivation is effective to passivate SiGe optical modulators for which low temperature processes are required.

OCIS codes: (130.3120) Integrated optics devices; (250.7360) Waveguide modulators.

References and links

1. G. T. Reed, G. Mashanovich, F. Y. Gardes, and D. J. Thomson, "Silicon optical modulators," Nat. Photonics **4**(8), 518–526 (2010).
2. R. A. Soref and B. R. Bennett, "Electrooptical Effects in Silicon," IEEE J Quantum Electron. **23**(1), 123–129 (1987).
3. Q. Xu, B. Schmidt, S. Pradhan, and M. Lipson, "Micrometre-scale silicon electro-optic modulator," Nature **435**(7040), 325–327 (2005).
4. Q. Xu, S. Manipatruni, B. Schmidt, J. Shakya, and M. Lipson, "12.5 Gbit/s carrier-injection-based silicon micro-ring silicon modulators," Opt. Express **15**(2), 430–436 (2007).
5. W. M. J. Green, M. J. Rooks, L. Sekaric, and Y. A. Vlasov, "Ultra-compact, low RF power, 10 Gb/s silicon Mach-Zehnder modulator," Opt. Express **15**(25), 17106–17113 (2007).
6. S. Akiyama, T. Baba, M. Imai, T. Akagawa, M. Takahashi, N. Hirayama, H. Takahashi, Y. Noguchi, H. Okayama, T. Horikawa, and T. Usuki, "12.5-Gb/s operation with 0.29-V·cm V(π)L using silicon Mach-Zehnder modulator based-on forward-biased pin diode," Opt. Express **20**(3), 2911–2923 (2012).
7. L. Liao, A. Liu, D. Rubin, J. Basak, Y. Chetrit, H. Nguyen, R. Cohen, N. Izhaky, and M. Paniccia, "40 Gbit/s silicon optical modulator for high-speed applications," Electron. Lett. **43**, 51–52 (2009).
8. D. J. Thomson, F. Y. Gardes, Y. Hu, G. Mashanovich, M. Fournier, P. Grosse, J. M. Fedeli, and G. T. Reed, "High contrast 40Gbit/s optical modulation in silicon," Opt. Express **19**(12), 11507–11516 (2011).
9. F. Y. Gardes, D. J. Thomson, N. G. Emerson, and G. T. Reed, "40 Gb/s silicon photonics modulator for TE and TM polarisations," Opt. Express **19**(12), 11804–11814 (2011).
10. T. Baehr-Jones, R. Ding, Y. Liu, A. Ayazi, T. Pinguet, N. C. Harris, M. Streshinsky, P. Lee, Y. Zhang, A. E.-J. Lim, T.-Y. Liow, S. H.-G. Teo, G.-Q. Lo, and M. Hochberg, "Ultralow drive voltage silicon traveling-wave modulator," Opt. Express **20**(11), 12014–12020 (2012).
11. J. Ding, R. Ji, L. Zhang, and L. Yang, "Electro-optical response analysis of a 40 Gb/s silicon Mach-Zehnder optical modulator," J. Lightwave Technol. **31**(14), 2434–2440 (2013).
12. M. Streshinsky, A. Ayazi, Z. Xuan, A. E.-J. Lim, G.-Q. Lo, T. Baehr-Jones, and M. Hochberg, "Highly linear silicon traveling wave Mach-Zehnder carrier depletion modulator based on differential drive," Opt. Express **21**(3), 3818–3825 (2013).
13. M. Streshinsky, R. Ding, Y. Liu, A. Novack, Y. Yang, Y. Ma, X. Tu, E. K. Chee, A. E. Lim, P. G. Lo, T. Baehr-Jones, and M. Hochberg, "Low power 50 Gb/s silicon traveling wave Mach-Zehnder modulator near 1300 nm," Opt. Express **21**(25), 30350–30357 (2013).

#205191 - $15.00 USD Received 21 Jan 2014; revised 12 Mar 2014; accepted 18 Mar 2014; published 24 Mar 2014

14. L. Yang and J. F. Ding, "High-Speed Silicon Mach-Zehnder Optical Modulator With Large Optical Bandwidth," J. Lightwave Technol. **32**(5), 966–970 (2014).
15. A. S. Liu, R. Jones, L. Liao, D. Samara-Rubio, D. Rubin, O. Cohen, R. Nicolaescu, and M. Paniccia, "A high-speed silicon optical modulator based on a metal-oxide-semiconductor capacitor," Nature **427**(6975), 615–618 (2004).
16. M. Takenaka and S. Takagi, "Strain Engineering of Plasma Dispersion Effect for SiGe Optical Modulators," IEEE J. Quantum Electron. **48**(1), 8–16 (2012).
17. J. Han, R. Zhang, T. Osada, M. Hata, M. Takenaka, and S. Takagi, "Improvement of SiGe MOS interfaces by plasma post-nitridation for SiGe high-k MOS optical modulators, ". 2012 IEEE International Conference on Group IV Photonics.
18. Y. Kim, M. Yokoyama, N. Taoka, M. Takenaka, and S. Takagi, "Ge-rich SiGe-on-insulator for waveguide optical modulator application fabricated by Ge condensation and SiGe regrowth," Opt. Express **21**(17), 19615–19623 (2013).
19. Y. Kim, M. Takenaka, and S. Takagi, "Numerical analysis of strained SiGe-based carrier-injection optical modulators," 2012 IEEE International Conference on Group IV Photonics.
20. Y. Kim, M. Takenaka, T. Osada, M. Hata, and S. Takagi, "Strain-induced enhancement of plasma dispersion effect and free-carrier absorption in SiGe optical modulators," eprint http://arXiv:1304.1229.
21. G. R. Zhou, M. W. Geis, S. J. Spector, F. Gan, M. E. Grein, R. T. Schulein, J. S. Orcutt, J. U. Yoon, D. M. Lennon, T. M. Lyszczarz, E. P. Ippen, and F. X. Käertner, "Effect of carrier lifetime on forward-biased silicon Mach-Zehnder modulators," Opt. Express **16**(8), 5218–5226 (2008).
22. S. Park, K. Yamada, T. Tsuchizawa, T. Watanabe, H. Shinojima, H. Nishi, R. Kou, and S. Itabashi, "Influence of carrier lifetime on performance of silicon p-i-n variable optical attenuators fabricated on submicrometer rib waveguides," Opt. Express **18**(11), 11282–11291 (2010).
23. R. Hull, J. C. Bean, D. J. Werder, and R. E. Leibenguth, "In situ observations of misfit dislocation propagation in Ge_xSi_{1-x}/Si(100) heterostructures," Appl. Phys. Lett. **52**(19), 1605 (1988).
24. Eh. Nicollia and A. Goetzber, "Si-SiO_2 Interface - Electrical Properties as Determined by Metal-Insulator-Silicon Conductance Technique," AT&T Tech. J. **46**, 1055 -& (1967).

1. Introduction

Si-based optical modulators have been attracted much attention as an essential component for on-chip optical interconnect in conjunction with electronics [1]. The Si optical modulators based on the plasma dispersion effect have been demonstrated [2] by means of carrier injection [3–6], depletion [7–14], and accumulation [15] using p-i-n, p-n, junctions, and MOS capacitor. However, the weak free-carrier effects in Si cause the low modulation efficiency, resulting in the longer device length [9]. The plasma dispersion effect and free-carrier absorption are expressed by the Drude model. According to the Drude model, the changes in refractive index and absorption coefficient are described by a change in the plasma frequency of free carriers, and the plasma frequency is dependent on not only the number of free carriers but also their conductivity effective masses. The change in the refractive index induced by the plasma dispersion effect is inversely proportional to the conductivity effective masses of electrons and holes [16–18]. Therefore, the lighter the conductivity masses become, the greater the plasma dispersion is. In terms of that, we have proposed carrier injection type SiGe modulator in which the plasma dispersion effect is enhanced by introducing a compressively strained SiGe layer as shown in Fig. 1 [19,20].

On the other hand, it is known that the modulation efficiency of the carrier injection type modulators is deteriorated by surface recombination due to interface traps between Si and a passivation layer. When carriers are injected to a waveguide core from p + and n + regions by forward bias, the injected carriers are trapped by interface traps, and recombined at dry-etched Si surfaces, decreasing carrier concentrations in the waveguide core where the light interacts with carriers [21,22]. A thermally grown SiO_2 layer is one of the best solutions for passivating etched Si surfaces with low interface trap densities; however it requires the high temperature oxidation process above 900 °C, which causes undesirable strain relaxation of strained SiGe [23]. Thus, a low temperature surface passivation process is indispensable for the strained SiGe optical modulators.

In this paper, we investigate a low temperature passivation process by using Al_2O_3 deposited by atomic layer deposition (ALD) to suppress surface recombination by using Si optical modulators. If SiGe modulators were used, we had to take into account the Ge diffusion impact on the modulation efficiency. Thus, it might be difficult to evaluate the surface passivation effect independently. Since interface traps on the etched Si slab region

#205191 - $15.00 USD Received 21 Jan 2014; revised 12 Mar 2014; accepted 18 Mar 2014; published 24 Mar 2014

mainly degrade the efficiency of carrier injection in both cases of Si and SiGe modulators, Si modulators are more preferable to investigate the surface passivation effect between the thermally grown SiO_2 and Al_2O_3. Evaluation of interface traps by *Capacitance-Voltage* (*C-V*) measurements of metal-oxide-semiconductor (MOS) capacitors reveals that Al_2O_3 passivation is effective to reduce the interface traps even with 200 °C process temperature. By introducing Al_2O_3 passivation prior to SiO_2 passivation, we demonstrate the improvement in the modulation efficiency of a carrier-injection Si optical modulator.

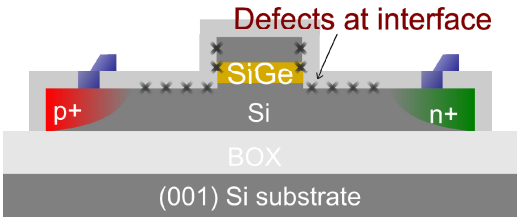

Fig. 1. Schematic device structure of carrier injection type strained SiGe optical modulator.

2. Evaluation of interface traps

To evaluate Al_2O_3 passivation effect, we have fabricated Al/Al_2O_3/Si MOS capacitors by ALD. A B-doped *p*-Si (N_A ~1 × 10^{15} cm^{-3}) substrate was used to fabricate the MOS capacitors. We have also fabricated Al/Al_2O_3/etched Si MOS capacitors to investigate interface traps generated by reactive ion etching (RIE) of Si surfaces. For comparison, Al/SiO_2/Si and etched Si MOS capacitors have also been fabricated by SiO_2 deposition by plasma enhanced chemical vapor deposition (PECVD). The interface trap density (D_{it}) distributions of the MOS capacitors are evaluated by the *C-V* measurements. Figure 2 shows the process flow of Al/Al_2O_3/etched Si MOS capacitor. First, the Si substrate was etched by RIE with CF_4 gas after organic cleaning. After cleaning Si surfaces by buffered HF, the 5-nm-thick Al_2O_3 was deposited at 200 °C. Then, Al electrode was formed by thermal evaporation. Finally, the forming gas annealing (FGA) was carried out for 30 min at 400 °C. Although a 1-nm thick Al_2O_3 layer is enough for passivating the Si surface, it is difficult to evaluate *C-V* curves when the Al_2O_3 thickness is less than 3 nm because of gate leakage current through quantum tunneling. Thus, we chose 5-nm thickness in Al_2O_3 to evaluate the interfacial properties by *C-V* measurements. The Al/SiO_2/etched Si MOS capacitor was fabricated by 45-nm-thick SiO_2 deposition at 350 °C instead of Al_2O_3. Since it is difficult to deposit 5-nm SiO_2 with keeping good uniformity, we chose 45-nm thickness in PECVD SiO_2. The difference in thickness between Al_2O_3 and SiO_2 does not affect the evaluation of interface trap density.

Since there are many interface traps at the PECVD SiO_2/Si interface, an additional annealing for 30 min at 1000 °C in N_2 was carried out after SiO_2 deposition.

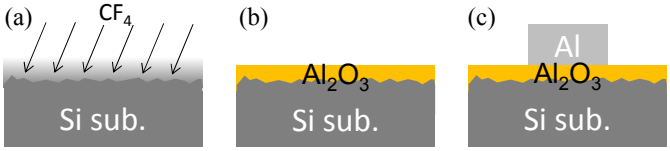

Fig. 2. Process flow of Al/Al_2O_3/etched Si MOS capacitor. (a) Dry etching, (b) Deposition of 5-nm-thick Al_2O_3 (c) Gate formation by Al electrode.

#205191 - $15.00 USD Received 21 Jan 2014; revised 12 Mar 2014; accepted 18 Mar 2014; published 24 Mar 2014

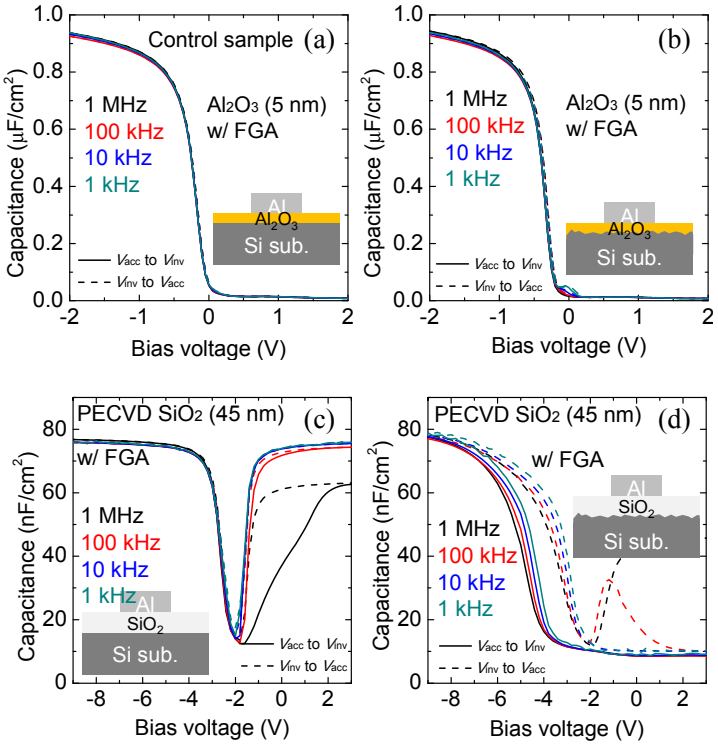

Fig. 3. *C-V* characteristics of (a) Al_2O_3/Si, (b) Al_2O_3/etched Si, (c) SiO_2/Si, and (d) SiO_2/etched Si MOS capacitors.

To investigate electrical properties of the MOS interfaces, we measured the *C-V* curves of the MOS capacitors at 1 kHz to 1 MHz. Figures 3 show the *C-V* characteristics of (a) the Al/Al_2O_3/Si, (b) the Al/Al_2O_3/etched Si, (c) Al/SiO_2/Si, and (d) Al/SiO_2/etched Si MOS capacitors. The solid line and dotted line show the voltage sweep of accumulation (V_{acc}) to inversion (V_{inv}) and inversion to accumulation, respectively. The *C-V* curves of the Al/Al_2O_3/Si MOS capacitor shows a well-behaved characteristic with no frequency dispersion, meaning that ALD Al_2O_3 can passivate Si surfaces well. It is found in Fig. 3(b) that the etched Si surface is also well passivated by Al_2O_3. On the other hand, Figs. 3(c) and (d) reveal that PECVD SiO_2 cannot passivate the etched Si surface because the Al/SiO_2/etched Si MOS capacitor exhibits stretch-out *C-V* curves with large frequency dispersion and hysteresis due to interface traps. Hence, it is shown that Al_2O_3 passivation is more effective to minimize etching damage of the Si surface than PECVD SiO_2 passivation. For the quantitative estimation, the energy distributions of D_{it} evaluated by the conductance method [24] are shown in Fig. 4. Although the etched Si samples exhibits higher D_{it} than the bulk Si sample, the ALD Al_2O_3 passivated surface shows D_{it} of less than 2×10^{11} cm^{-2} eV^{-1}. On the other hand, the PECVD SiO_2 passivated surface has D_{it} of larger than 10^{12} $cm^{-2}eV^{-1}$. Hence, the Al_2O_3 passivation is more effective to suppress surface recombination due to low interface traps.

#205191 - $15.00 USD Received 21 Jan 2014; revised 12 Mar 2014; accepted 18 Mar 2014; published 24 Mar 2014

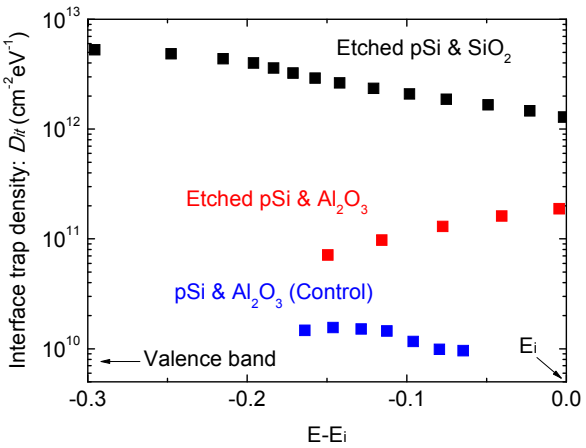

Fig. 4. Interface trap density distributions of the SiO_2/etched Si, the Al_2O_3/etched Si, and the Al_2O_3/Si MOS interfaces.

3. Device fabrication and characterization

To evaluate the effect of surface passivation on the modulation characteristics, the pin-junction-based in-line optical modulators with the Al_2O_3 or SiO_2 passivation were fabricated by using a 220-nm-thick silicon-on-insulator (SOI) with N_A of ~1×10^{15} cm^{-3} wafer as shown in Fig. 5. To estimate carrier injection efficiency precisely, it is necessary to evaluate the modulator characteristic in the wide range of injection current. However, it is not easy to precisely estimate the carrier injection efficiency from refractive index change in a Mach-Zehnder interferometer (MZI) due to the unavoidable free-carrier absorption in an MZI's arm which degrades interference properties. In the case of an in-line modulator, there is not such a problem to evaluate attenuation properties in the wide range of injection current. Therefore, an in-line modulator based on straight waveguide was used for the attenuation characteristics. First, the straight rib waveguide was formed by deep ultraviolet lithography and dry etching by reactive ion etching with CF_4 gas, followed by 20-nm-thick SiO_2 deposition by PECVD as a hard mask in Fig. 5(a). The width and mesa of waveguide is 2 μm and 120 nm, respectively. We chose the width of waveguides for obtaining enough optical output power in the experiments. Since we fabricated the waveguide by using contact photolithography, the propagation loss is large when the waveguide width is less than 1 μm due to the large sidewall roughness. In addition, the coupling loss is increased by narrowing waveguide width due to end coupling. The 2-μm-wide waveguide has theoretically high-order optical modes. However, we have tried to couple the light to the fundamental mode of the 2-μm-wide waveguide as much as possible by monitoring the output image through InGaAs camera. Thus, the 2-μm-wide waveguide does not have significant impact on evaluating the attenuation properties. Although the waveguide width should be scaled down to 500 nm for high speed operation, we have focused on carrier injection efficiency which is affected by interface traps on the Si surfaces. Therefore, it is not a significant matter to use the 2-μm-wide waveguide for evaluating the static characteristics of output power by carrier injection in this paper. Then, ion implantations of boron and phosphorus (dose: 1×10^{15} cm^{-2}, energy: 10 keV and 30 keV, respectively) were carried out to make the p + and n + regions to form a lateral pin-junction, followed by activation annealing at 1000 °C for 30 min in N_2 atmosphere in Fig. 5(b). Here, the distance between implanted regions and waveguide edge is approximately 2 μm. Then, the contact pads for the p + and n + regions were formed by thermal evaporation of aluminum. The final structure of a SiO_2-passivated device is shown in Fig. 4(c). In the case of the Al_2O_3-passivated device, the SiO_2 passivation layer was removed by wet etching using BHF after activating the implanted dopants. Then, a 1-nm-thick Al_2O_3 layer was deposited on

#205191 - $15.00 USD Received 21 Jan 2014; revised 12 Mar 2014; accepted 18 Mar 2014; published 24 Mar 2014

Si as a passivation layer by ALD at 200 °C and a 280-nm-thick SiO_2 layer was deposited on Al_2O_3 layer by PECVD as shown in Fig. 5(e). Finally, the contact pads regions were formed. The final structure of a Al_2O_3 passivated device is shown in Fig. 5(f). Forming gas annealing was implemented for all devices to decrease the contact resistance, which is for 30 min at 400 °C. Figure 6 shows a top-view of the fabricated device passivated by Al_2O_3. The structure of in-line modulator has been used to estimate the optical attenuation occurred by free-carrier absorption.

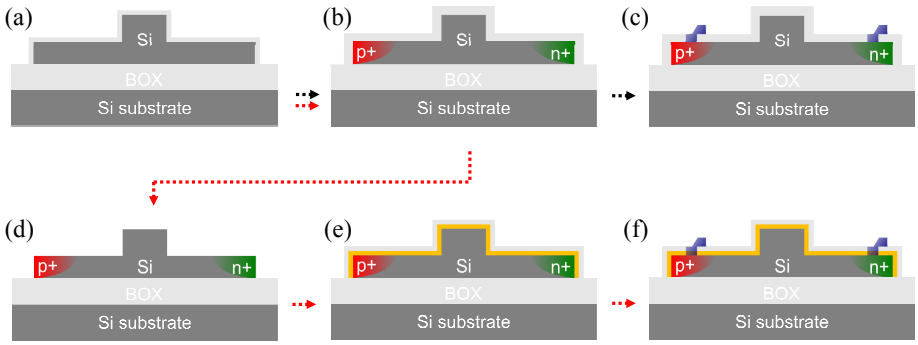

Fig. 5. Process flow of carrier-injection type Si in-line optical modulator. (a) Waveguide formation (b) p + and n + region formation by ion implantation and activation. (c) Final structure of SiO_2-passivated device after Al electrode formation, (d) Removal of SiO_2 passivation layer by wet etching (e) Al_2O_3 and SiO_2 passivation, and (f) Final structure of Al_2O_3-passivated device after Al electrode formation

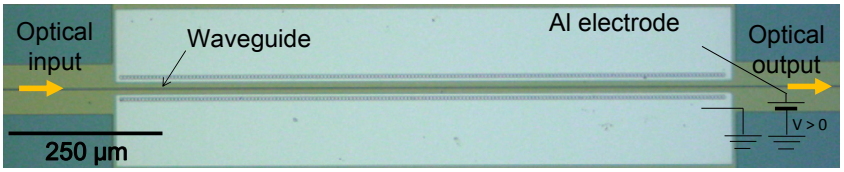

Fig. 6. Top-view of Al_2O_3-passivated device observed by optical microscopy.

Figure 7 shows the measured optical attenuation properties of the Si in-line intensity modulators with and without the Al_2O_3 layer as a function of injected current. The optical attenuation was measured by injecting current to evaluate the effect of Al_2O_3 passivation. Since we have not focused on high-speed operation, the static characteristics of attenuation are measured to evaluate the carrier injection efficiency. Continuous-wave (CW) TE-polarized light with a wavelength of 1550 nm was coupled to the waveguide through a lensed fiber. Then, the output power was monitored using an InGaAs photodetector while changing the injection current. The length of the phase-shifters is 1 mm. It can be seen that the attenuation of the Al_2O_3-passivated modulator is larger than that of the SiO_2-passivated modulator. As a result, the injection current required for the 20-dB attenuation can be reduced from 64 mA/mm to 47 mA/mm owing to the reduction in the interface trap density using the Al_2O_3 passivation layer. Also, we have fabricated the Si in-line intensity modulator passivated by the thermally oxidized SiO_2 at 1000 °C. It is worth noting that the performance of the Al_2O_3-passivated device is comparable to the SiO_2 passivated device formed by dry oxidation, indicating that Al_2O_3 passivation is as good as SiO_2 passivation by dry oxidation in terms of surface recombination. We can estimate the modulation efficiency in $V_\pi L$ from the attenuation results. Since the voltage necessary for 20-dB attenuation is reduced from 2.2 V to 1.8 V by using Al_2O_3 passivation as compared with PECVD SiO_2 passivation, $V_\pi L$ of the Al_2O_2-passivated device is expected to be improved by approximately 20%, which is comparable to the thermally grown SiO_2 passivation. We have also found no significant

#205191 - $15.00 USD Received 21 Jan 2014; revised 12 Mar 2014; accepted 18 Mar 2014; published 24 Mar 2014

impact of the passivation layers on the propagation loss. Thus, the total insertion loss is not changed even in the Al_2O_3-passivated device.

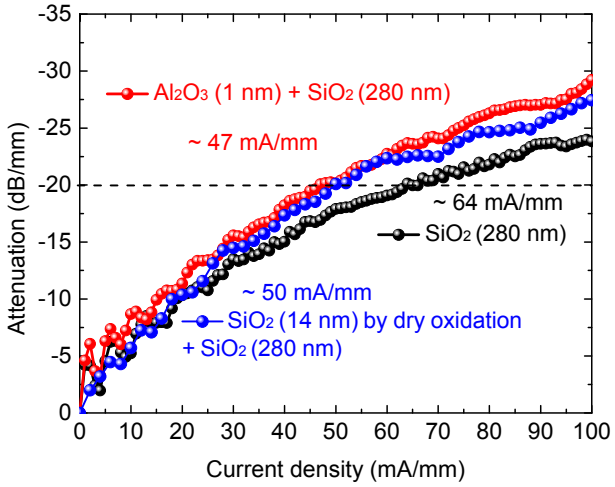

Fig. 7. Attenuation characteristics of Si modulators passivated by PECVD SiO_2 (black), dry-oxidized SiO_2 (blue), and Al_2O_3 (red).

6. Conclusion

We have investigated the low-temperature surface passivation, which is especially necessary for carrier-injection SiGe optical modulators due to the restriction of thermal budge, for suppressing surface recombination. We find that Al_2O_3 passivation formed by ALD at 200 °C is effective to decrease interface traps on the etched Si surfaces at low temperature as compared with PECVD SiO_2 passivation. The interface trap density of the Al_2O_3-passivated etched Si surface is less than 2×10^{11} $cm^{-2}eV^{-2}$, which is one order magnitude lower than that of the PECVD SiO_2-passivated surface. The modulation efficiency is also improved by introducing the Al_2O_3 passivation layer prior to SiO_2 deposition. The injection current density for 20-dB attenuation is improved by approximately 40%, which is comparable to the thermally grown SiO_2-passivated device. Thus, ALD Al_2O_3 is promising for passivating the strained SiGe optical modulator at low temperature.

Acknowledgments

This work was partly supported by the Strategic Information and Communications R&D Promotion Programme of the Ministry of Internal Affairs and Communications.

#205191 - $15.00 USD Received 21 Jan 2014; revised 12 Mar 2014; accepted 18 Mar 2014; published 24 Mar 2014